ACS Energy LETTERS

http://pubs.acs.org/journal/aelccp

LETTER

# Optimization of Stable Quasi-Cubic $FA_xMA_{1-x}PbI_3$ Perovskite Structure for Solar Cells with Efficiency beyond 20%

Yi Zhang,[†,‡] Giulia Grancini,[*,†] Yaqing Feng,[‡] Abdullah M. Asiri,[§] and Mohammad Khaja Nazeeruddin[*,†]

[†]Group for Molecular Engineering of Functional Materials, EPFL Valais Wallis, CH-1951 Sion, Switzerland

[‡]School of Chemical Engineering and Technology, Tianjin University, Tianjin 300072, China

[§]Center of Excellence for Advanced Materials Research (CEAMR), King Abdulaziz University, Jeddah, Saudi Arabia

Supporting Information

**ABSTRACT: Complex compositional engineering of mixed halides/mixed cations perovskites has recently fostered a rapid progress in perovskite solar cell technology. Here we demonstrate that when 10% of formamidinium ($FA^+$) is simply added into methylammonium lead iodide ($MAPbI_3$) a highly crystalline and compositionally uniform perovskite is formed, self-organizing into a stable "quasi-cubic" phase at room temperature. We reached power conversion efficiency of over 20.2%, the highest value reported to date for $FA_xMA_{1-x}PbI_3$ perovskite.**

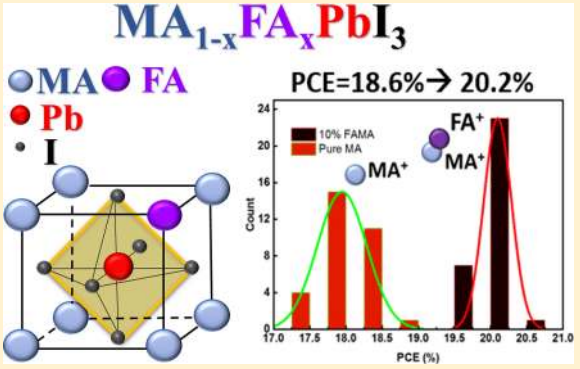


Hybrid perovskite technology with astonishing power conversion efficiency (PCE) beyond 22% promises to be an ideal candidate for near future solar power generation.[1−4] Beyond their excellent optoelectronic properties[5,6] and ease, versatility, and low cost in the processing techniques,[7] the ability of the perovskite to accommodate different cations and anions within the lattice gives room for a myriad of different material combinations.[2,3] The incorporation of methylammonium ($MA^+$), formamidinium ($FA^+$), cesium ($Cs^+$), and rubidium ($Rb^+$) along with a mixture of Cl, Br, and I halides enabled the fabrication of high-efficiency solar cells with, in some cases, improved stability.[3,7] Additionally, ion intermixing enables a fine-tuning of the material bandgap with direct impact on tandem solar cell engineering.[2] However, as a drawback, compositional engineering induces severe changes in the crystal structure and film morphology associated with halide phase segregation[7,8] and light/field-induced ion movement[9−12] altering the device function. Interestingly, the inclusion of $Cs^+$ has been shown to enhance device stability.[4,9] However, the added complexity of the material structure and the difficulties in reproducing the performances casts the doubt on the ease of reproducibility and scale-up of this route. On the other side, a much simpler structure in which only FA is introduced with MA as the organic compound leaving intact the inorganic backbone has attracted a great deal of interest.[10−13] FA-based perovskite has shown a superior stability compared to that of the methylammonium, longer charge diffusion length, and a band gap closer to the ideal value.[2,7,7,9,11,11,13−16] However, the larger radii of the FA cation disturbs the formation of a stable $\alpha$ phase and high-quality $FAMAPbI_3$ film, especially when a large percentage of FA is used (note that pure $FAPbI_3$ undergoes a phase transition to yellow nonperovskite $\delta$-$FAPbI_3$[12]).[7,10] This, in turn, has limited to date the device performances of $FA_xMA_{1-x}PbI_3$ to 15−16% because of the poor crystallization of the resulting film.[17−19] In this study we found that by using a small amount of FA (between 10 and 30%) in the $MAPbI_3$ perovskite processed by a one-step deposition method followed by solvent engineering step, a high-quality crystal film can be obtained. By means of structural and optical characterization we found that the $FA^+$ intercalates with the $MA^+$ within the voids of the $PbI_6$ octahedra, stabilizing the perovskite structure into a "quasi-cubic" phase at room temperature. We fabricated solar devices where the perovskite is sandwiched between the 2,2′,7,7′-tetrakis(*N*,*N*-dipmethoxyphenylamine)-9,9′-spirobifluorene (spiro-OMeTAD) hole-transporting material and the mesoscopic $TiO_2$ scaffold (m-$TiO_2$) electron transporter in a standard architecture.[3,20] The results show a significant step

**Received:** February 7, 2017
**Accepted:** March 9, 2017

 © XXXX American Chemical Society 

DOI: 10.1021/acsenergylett.7b00112
*ACS Energy Lett.* 2017, 2, 802−806

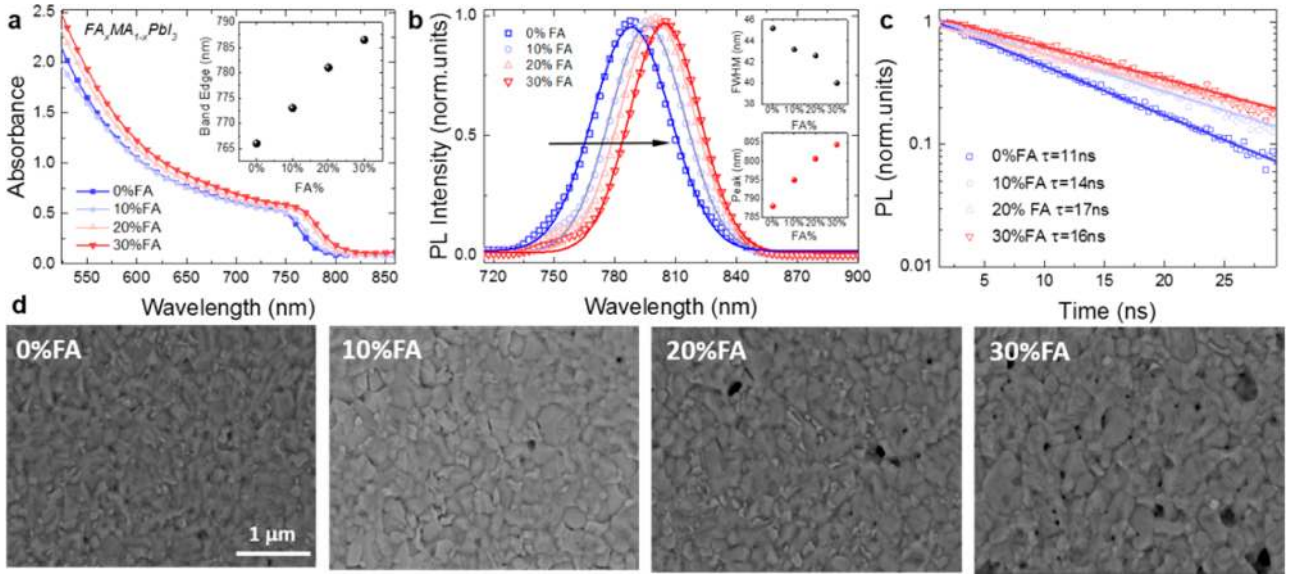


**Figure 1.** (a) Absorption spectra of $FA_xMA_{1-x}PbI_3$ films ($x$ = 0, 10%, 20%, 30%). Inset: band edge position as a function of FA%. (b) PL spectra of $FA_xMA_{1-x}PbI_3$ films ($x$ = 0, 10%, 20%, 30%) excitation at 460 nm. Insets: (top) fwhm of the PL spectra retrieved from single-peak fitting and (bottom) peak position as a function of FA%. (c) PL decay upon excitation at 460 nm at excitation density of <1 nJ/cm$^2$ corresponding to an average density of absorbed photons of $10^{16}$ photons/cm$^3$. The films have been encapsulated to prevent degradation or any oxygen- or moisture-induced effects. (d) SEM top-view images of the $FA_xMA_{1-x}PbI_3$ films ($x$ = 0, 10%, 20%, 30%). Scalebar: 1 $\mu$m.

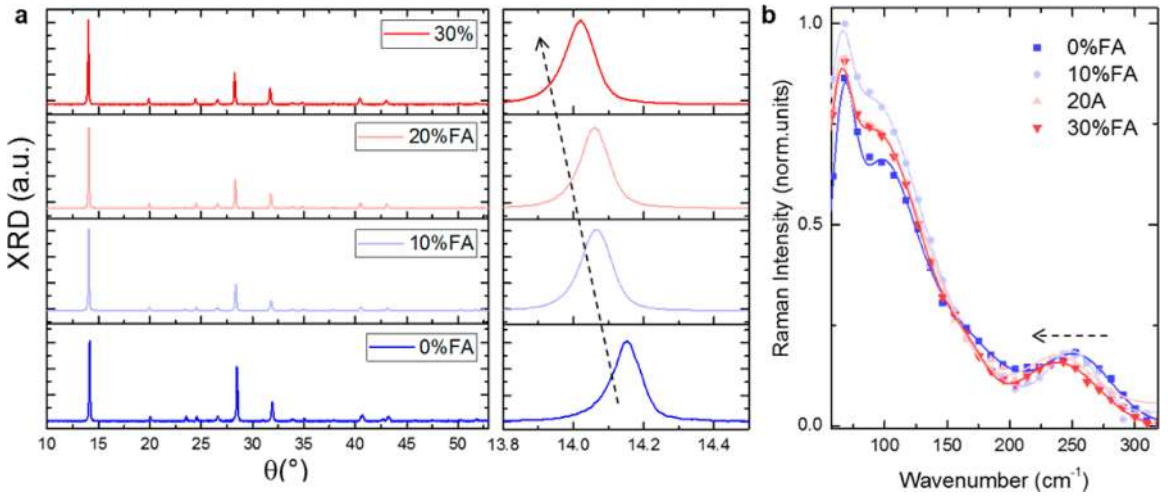


**Figure 2.** (a) X-ray diffraction spectra of $FA_xMA_{1-x}PbI_3$ films ($x$ = 0, 10%, 20%, 30%) along with a zoomed-in view of the peak at 14°. (b) Raman spectra of $FA_xMA_{1-x}PbI_3$ films ($x$ = 0, 10%, 20%, 30%).

forward in device efficiency, with champion device showing PCE > 20.2% accompanied by a very good statistics on device performance and hysteresis-free behavior. Such performances, not far from that obtained with much more complicated structures which incorporate many different compound, can be obtained with a much simpler and highly reproducible protocol. This is of the utmost importance for the scale-up and future commercialization of this technology.

Figure 1a shows the absorption spectra of the mixed cation lead iodide perovskites $FA_xMA_{1-x}PbI_3$ at different FA percentage (from 0 to 30%). When the amount of FA% is increased, the absorption onset experiences a red-shift of around 25 nm, as shown in the inset. The normalized photoluminescence (PL) spectra are reported in Figure 1b. In agreement, a significant red-shift in the emission peak of $FA_xMA_{1-x}PbI_3$ is observed upon increasing $x$. In addition, a reduction of the broadening of the peak is measured (see the inset of Figure 1b). The gradual shift derives from the intermixing of FA and MA in the perovskite lattice, while the reduced inhomogeneous broadening can suggest a higher crystallinity, with the increasing FA% associated with lower energetic disorder with respect to the pure $MAPbI_3$.[7,21] Figure 1c reports the time-resolved PL. The dynamical radiative decay is here monitored to better understand the influence of the perovskite composition, i.e. the addition of FA, on the carrier dynamics.

Measurements are performed using time-correlated single-photon counting (TCSPC) under low-intensity pulsed excitation at 460 nm at <1 nJ/cm$^2$, close to the typical solar light flux.[6] At this intensity, the photoexcited carrier densities are expected to be low and trap-mediated recombination is likely the dominant decay pathway. In this regime we observe that the decay processes can be well fit by monoexponential profiles with PL lifetimes increasing from 10 to 17 ns with



DOI: 10.1021/acsenergylett.7b00112
ACS Energy Lett. 2017, 2, 802−806

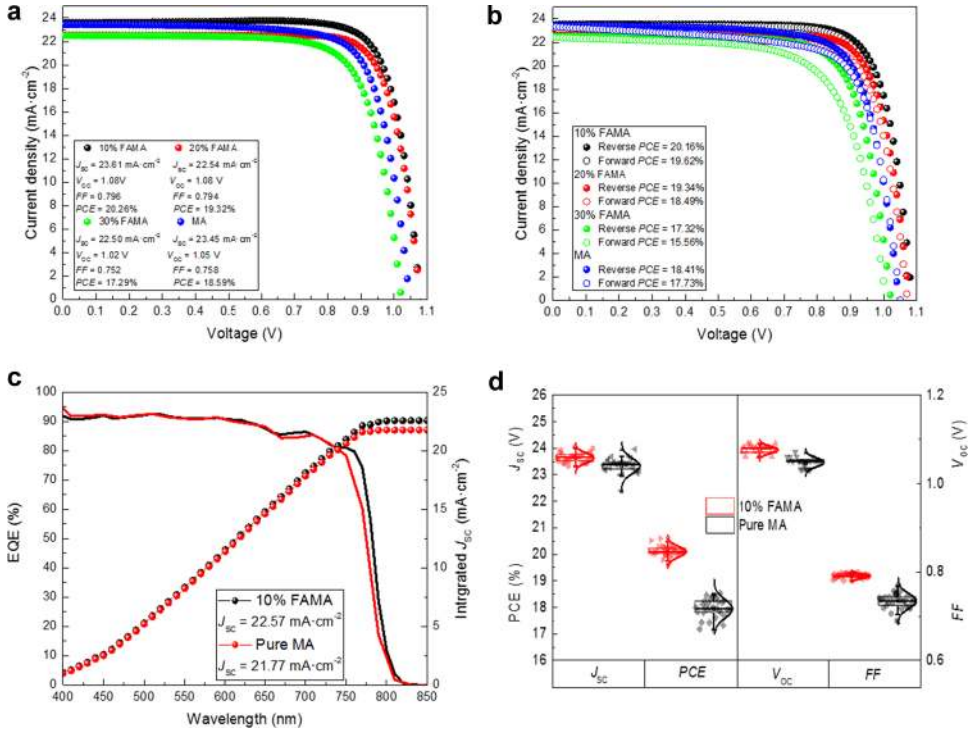


**Figure 3. (a) Current density−voltage ($J$−$V$) curves and parameters of $FA_xMA_{1-x}PbI_3$ ($x$ = 0, 10%, 20%, 30%) devices including (b) the $J$−$V$ curve hysteresis, (c) EQE and corresponding integrated JSC of the devices comparing 0% FA with 10% FA, and (d) distribution of the device parameters comparing 40 devices with 0% and 10% FA.**

increasing FA%. The monoexponential decay can be associated with monomolecular and trap-mediated recombination.[7,14,22] This observed dependence of PL decay dynamics on composition suggests that with increasing FA% the crystallinity is enhanced, leading to reduced charge trapping or improved carrier diffusion length, as suggested in refs 7 and 14. Note also that a longer PL lifetime has been measured when the perovskite organizes into a stable cubic structure.[10,14] (See also Figure S1, which reports the calculated rate (as 1/time constant) as a function of FA%.) Figure 1d shows the SEM top image of the films investigated. Notably, as the FA% increases, the average size of the grains increases (see also the calculated averaged values in Figure S2) going from 160 nm for 0% FA to 300 nm for 30% FA. However, one could note that when FA% > 20% the films show the presence of large darker regions possibly due to thinner areas or pinholes resulting from a nonuniform growth. Figure 2 shows the X-ray diffraction (XRD) patterns of the mixed cation perovskites developed. With respect to the pure $MAPbI_3$, the introduction of the large $FA^+$ cation with the smaller $MA^+$ decreases the tolerance factor and induces the formation of a stable cubic perovskite phase.[10,13,17,22−24] Depending on film morphology and deposition conditions, adding a small amount of FA (such as 10%) might lead to a tetragonal phase as observed when the film is formed by precipitation from aqueous hydroiodic acid.[24] In our case, we observe that the peak position of the diffraction peaks at 14.1 (see also the zoomed-in views), 20.0, 24.4, 28.4, and 31.8 decrease with increasing FA%, which enlarges the crystal lattice going to a cubic or "quasi-cubic" crystal phase. The gradual shift in the diffraction angle further confirms that in the mixed $FA_xMA_{1-x}PbI_3$ the two cations are copresent in the perovskite lattice, stabilizing the perovskite in a "quasi cubic" phase. Figure 2a further shows the zoomed (100) diffraction peak at $2\theta \approx 14°$, which continuously shifts to 13.86° as the FA% increases. Note also that the peaks related to pure $FAPbI_3$ or $MAPbI_3$ phases are not present. This further supports the fine intermixing of the cations in the mixed perovskite without inducing the phase segregation within the film. Figure 2b shows the Raman spectrum of the mixed $FA_xMA_{1-x}PbI_3$ perovskite films, here reported for the first time. The Raman spectra consist of four main peaks (see additional data reported in Table S1). Similarly to the pristine $MAPbI_3$ perovskite (see also Figure S3), the peaks below 150 $cm^{-1}$ reflect the Pb−I vibrations representing a combination of the Pb−I stretching and bending modes along with a minor contribution of the organic cations previously identified at 129 $cm^{-1}$.[8,25−27] On the other side, the peak at higher wavenumber relates to the torsion of the organic cations.[8] In particular, this peak has been measured and calculated to be around 230 $cm^{-1}$ for the pure FA torsional mode, being on the other side shifted to 290 $cm^{-1}$ for the pure MA torsion[8,26,27] (see also Figure S3). From the analysis of this spectral region for the mixed $FA_xMA_{1-x}PbI_3$, we observe that only one peak is observed that continuously red shifts with increasing the amount of FA%. Note that in the case of halide segregation, as recently demonstrated by a few of us,[8] two distinguishable peaks from the $FA^+$ and $MA^+$ torsions can be identified, while in this case only one mode is identified and is related to the cubic perovskite structure where FA and MA are combined together and do not form segregated perovskite phases.

Solar cells using 0−30% addition of FA have been fabricated and optimized. The current−voltage ($J$−$V$) characteristics of the solar cells under simulated air mass 1.5 global standard sunlight (AM1.5G) are reported in Figure 3a along with the device parameters. Champion devices show for the pure $MAPbI_3$ power conversion efficiency of 18.59%, in line with what has been reported in the literature for the pristine compound.[20] Solar cells with the addition of FA generally show



DOI: 10.1021/acsenergylett.7b00112
ACS Energy Lett. 2017, 2, 802−806

a higher open-circuit voltage ($V_{oc}$) and, for 10% FA, a significant improvement in the device PCE. The most efficient $FA_{0.1}MA_{0.9}PbI_3$-based device provides a PCE of 20.26%, outperforming the single-cation compositions $MAPbI_3$. Device statistics showing the parameters averaged on 30 devices are reported in Figure S4 along with the photovoltaic parameters in Table S2. This further confirms the statistically higher performances we could obtain with the addition of $FA_{0.1}MA_{0.9}PbI_3$. In Table 1 we report the PV characteristics

**Table 1. Photovoltaic Parameter of Short-Circuit Photocurrent Density ($J_{sc}$), Open-Circuit Voltage ($V_{oc}$), Fill Factor (FF), and Power Conversion Efficiency (PCE)**

| sample | $J_{sc}$ (mA cm$^{-2}$) | $V_{oc}$ (V) | FF | PCE (%) |
|---|---|---|---|---|
| $MAPbI_3$ | 23.45 | 1.05 | 0.758 | 18.59 |
| 10% FA | 23.61 | 1.08 | 0.796 | 20.26 |
| 20% FA | 22.54 | 1.08 | 0.794 | 19.32 |
| 30% FA | 22.50 | 1.02 | 0.752 | 17.29 |

of a series of cells with varying the FA%. Figure 3b shows the $J-V$ hysteresis of the cell (the corresponding photovoltaic parameters are listed in Table S3). The $FA_{0.1}MA_{0.9}PbI_3$ shows the lowest hysteresis factor, suggesting that adding 10%FA strongly stabilizes the structure, limiting any light- or field-induced ion movement and impeding the halide segregation. Note also that a stable device behavior is obtained after few seconds of illumination, upon which stable device parameters could be registered (see details in Figure S5 and in Table S4). Overall, this favors a stable device operation. Further details on the long-term stability of the device are reported in Figure S6. Similarly to the $MAPbI_3$, an initial decay is observed, possibly due to the interdiffusion of the gold top electrode.[28] However, over longer time, an improved long-term stability is registered at least for the first 300 h time lapse. The incident photon-to-current conversion efficiency (IPCE), or external quantum efficiency, across the visible spectrum is presented in Figure 3c. The photocurrent onset is shifted in the red for the $FA_{0.1}MA_{0.9}PbI_3$ device from 780 to 800 nm, providing a gain in the photocurrent. The higher $V_{oc}$ can correlate with the slightly larger band gap upon the introduction of FA. Integration of the IPCE spectra (340−850 nm) over the AM1.5G solar emission spectrum yielded short-circuit photocurrent densities of 22.57 and 21.77 mA·cm$^{-2}$ for $FA_{0.1}MA_{0.9}PbI_3$ and pure $MAPbI_3$, respectively. The statistics of the photovoltaic parameters obtained are reported in Figure 3d, showing that the results are statistically significant and reproducible, providing a strong proof of the concept presented here.

In conclusion, we have reported for the first time a simple and highly reproducible method for obtaining highly efficient hybrid perovskite solar cells by incorporating 10% of FA into the $MAPbI_3$ structure. The formation of a stable "quasi-cubic" phase at room temperature accompanied by improved crystal quality is the reason behind the high performances obtained. We envisage that, although a lot of work with promising results is ongoing on mixed halide perovskite including mixture of $Cs^+$ and $Rb^+$ as cations and iodine and bromide as anions, a much simpler and robust method, as the one here presented, can sustain the realization of >20% efficient device and, more importantly, open the way for the scale-up of the hybrid perovskite technology.

## ■ ASSOCIATED CONTENT

### Supporting Information

The Supporting Information is available free of charge on the ACS Publications website at DOI: 10.1021/acsenergylett.7b00112.

Additional data and details on the experimental methods (PDF)

## ■ AUTHOR INFORMATION


### Corresponding Authors

*E-mail: giulia.grancini@epfl.ch.

*E-mail: mdkhaja.nazeeruddin@epfl.ch.

### ORCID

Giulia Grancini: 0000-0001-8704-4222

Mohammad Khaja Nazeeruddin: 0000-0001-5955-4786


### Notes

The authors declare no competing financial interest.

## ■ ACKNOWLEDGMENTS

G.G. is supported by the cofunded Marie Skłodowska Curie fellowship, H2020 Grant agreement no. 665667, fund number 588072. This project was funded by the Deanship of Scientific Research (DSR), King Abdulaziz University, Jeddah, under Grant no. 79-130-35-HiCi. Y.Z. acknowledges the financial support of China Scholarship Council fellowship. The authors acknowledge Dr. Emad Oveisi of CIME-EPFL for SEM measurement and Manuel Tschumi for stability measurement.

## ■ REFERENCES


(1) Correa-Baena, J.-P.; Abate, A.; Saliba, M.; Tress, W.; Jacobsson, T. J.; Grätzel, M.; Hagfeldt, A. The rapid evolution of highly efficient perovskite solar cells. *Energy Environ. Sci.* **2017**, DOI: 10.1039/C6EE03397K.

(2) McMeekin, D. P.; Sadoughi, G.; Rehman, W.; Eperon, G. E.; Saliba, M.; Hörantner, M. T.; Haghighirad, A.; Sakai, N.; Korte, L.; Rech, B.; et al. A mixed-cation lead mixed-halide perovskite absorber for tandem solar cells. *Science* **2016**, *351*, 151−155.

(3) Saliba, M.; Matsui, T.; Domanski, K.; Seo, J.-Y.; Ummadisingu, A.; Zakeeruddin, S. M.; Correa-Baena, J.-P.; Tress, W. R.; Abate, A.; Hagfeldt, A.; et al. Incorporation of rubidium cations into perovskite solar cells improves photovoltaic performance. *Science* **2016**, *354*, 206−209.

(4) Zhang, Y.; Gao, P.; Oveisi, E.; Lee, Y.; Jeangros, Q.; Grancini, G.; Paek, S.; Feng, Y.; Nazeeruddin, M. K. $PbI_2$−HMPA Complex Pretreatment for Highly Reproducible and Efficient $CH_3NH_3PbI_3$ Perovskite Solar Cells. *J. Am. Chem. Soc.* **2016**, *138*, 14380−14387.

(5) Stranks, S. D.; Snaith, H. J. Metal-halide perovskites for photovoltaic and light-emitting devices. *Nat. Nanotechnol.* **2015**, *10*, 391−402.

(6) D'Innocenzo, V.; Grancini, G.; Alcocer, M. J.; Kandada, A. R. S.; Stranks, S. D.; Lee, M. M.; Lanzani, G.; Snaith, H. J.; Petrozza, A. Excitons versus free charges in organo-lead tri-halide perovskites. *Nat. Commun.* **2014**, *5*, 3586.

(7) Rehman, W.; McMeekin, D. P.; Patel, J. B.; Milot, R. L.; Johnston, M. B.; Snaith, H. J.; Herz, L. M. Photovoltaic mixed-cation lead mixed-halide perovskites: links between crystallinity, photostability and electronic properties. *Energy Environ. Sci.* **2017**, *10*, 361−369.

(8) Gratia, P.; Grancini, G.; Audinot, J.-N.; Jeanbourquin, X.; Mosconi, E.; Zimmermann, I.; Dowsett, D.; Lee, Y.; Grätzel, M.; De Angelis, F.; et al. Intrinsic Halide Segregation at Nanometer Scale Determines the High Efficiency of Mixed Cation/Mixed Halide Perovskite Solar Cells. *J. Am. Chem. Soc.* **2016**, *138*, 15821−15824.




DOI: 10.1021/acsenergylett.7b00112
*ACS Energy Lett.* 2017, 2, 802−806

(9) Lee, J.-W.; Kim, D.-H.; Kim, H.-S.; Seo, S.-W.; Cho, S. M.; Park, N.-G. Formamidinium and Cesium Hybridization for Photo- and Moisture-Stable Perovskite Solar Cell. *Adv. Energy Mater.* **2015**, *5*, 1501310.
(10) Binek, A.; Hanusch, F. C.; Docampo, P.; Bein, T. Stabilization of the Trigonal High-Temperature Phase of Formamidinium Lead Iodide. *J. Phys. Chem. Lett.* **2015**, *6*, 1249−1253.
(11) Chen, J.; Xu, J.; Xiao, L.; Zhang, B.; Dai, S.; Yao, J. Mixed-Organic-Cation $(FA)_x(MA)_{1-x}PbI_3$ Planar Perovskite Solar Cells with 16.48% Efficiency via a Low-Pressure Vapor-Assisted Solution Process. *ACS Appl. Mater. Interfaces* **2017**, *9*, 2449−2458.
(12) Ji, F.; Wang, L.; Pang, S.; Gao, P.; Xu, H.; Xie, G.; Zhang, J.; Cui, G. A balanced cation exchange reaction toward highly uniform and pure phase $FA_{1-x}MA_xPbI_3$ perovskite films. *J. Mater. Chem. A* **2016**, *4*, 14437−14443.
(13) Li, G.; Zhang, T.; Guo, N.; Xu, F.; Qian, X.; Zhao, Y. Ion-Exchange-Induced 2D−3D Conversion of $HMA_{1-x}FA_xPbI_3Cl$ Perovskite into a High-Quality $MA_{1-x}FA_xPbI_3$ Perovskite. *Angew. Chem., Int. Ed.* **2016**, *55*, 13460−13464.
(14) Dai, J.; Fu, Y.; Manger, L. H.; Rea, M. T.; Hwang, L.; Goldsmith, R. H.; Jin, S. Carrier Decay Properties of Mixed Cation Formamidinium−Methylammonium Lead Iodide Perovskite $[HC(NH_2)_2]_{1-x}[CH_3NH_3]_xPbI_3$ Nanorods. *J. Phys. Chem. Lett.* **2016**, *7*, 5036−5043.
(15) Salado, M.; Calio, L.; Berger, R.; Kazim, S.; Ahmad, S. Influence of the mixed organic cation ratio in lead iodide based perovskite on the performance of solar cells. *Phys. Chem. Chem. Phys.* **2016**, *18*, 27148−27157.
(16) Zhang, T.; Meng, X.; Bai, Y.; Xiao, S.; Hu, C.; Yang, Y.; Chen, H.; Yang, S. Profiling the organic cation-dependent degradation of organolead halide perovskite solar cells. *J. Mater. Chem. A* **2017**, *5*, 1103−1111.
(17) Pellet, N.; Gao, P.; Gregori, G.; Yang, T.-Y.; Nazeeruddin, M. K.; Maier, J.; Grätzel, M. Mixed-Organic-Cation Perovskite Photovoltaics for Enhanced Solar-Light Harvesting. *Angew. Chem., Int. Ed.* **2014**, *53*, 3151−3157.
(18) Liu, J.; Shirai, Y.; Yang, X.; Yue, Y.; Chen, W.; Wu, Y.; Islam, A.; Han, L. High-Quality Mixed-Organic-Cation Perovskites from a Phase-Pure Non-stoichiometric Intermediate $(FAI)_{1-x}$-$PbI_2$ for Solar Cells. *Adv. Mater.* **2015**, *27*, 4918−4923.
(19) Isikgor, F. H.; Li, B.; Zhu, H.; Xu, Q.; Ouyang, J. High performance planar perovskite solar cells with a perovskite of mixed organic cations and mixed halides, $MA_{1-x}FA_xPbI_{3-y}Cl_y$. *J. Mater. Chem. A* **2016**, *4*, 12543−12553.
(20) Roldan-Carmona, C.; Gratia, P.; Zimmermann, I.; Grancini, G.; Gao, P.; Graetzel, M.; Nazeeruddin, M. K. High efficiency methylammonium lead triiodide perovskite solar cells: the relevance of non-stoichiometric precursors. *Energy Environ. Sci.* **2015**, *8*, 3550−3556.
(21) Stranks, S. D.; Eperon, G. E.; Grancini, G.; Menelaou, C.; Alcocer, M. J.; Leijtens, T.; Herz, L. M.; Petrozza, A.; Snaith, H. J. Electron-hole diffusion lengths exceeding 1 micrometer in an organometal trihalide perovskite absorber. *Science* **2013**, *342*, 341−344.
(22) Matsui, T.; Seo, J.-Y.; Saliba, M.; Zakeeruddin, S. M.; Grätzel, M. Room-Temperature Formation of Highly Crystalline Multication Perovskites for Efficient, Low-Cost Solar Cells. *Adv. Mater.* **2017**, 1606258.
(23) Ma, F.; Li, J.; Li, W.; Lin, N.; Wang, L.; Qiao, J. Stable $\alpha/\delta$ phase junction of formamidinium lead iodide perovskites for enhanced near-infrared emission. *Chem. Sci.* **2017**, *8*, 800−805.
(24) Weber, O. J.; Charles, B.; Weller, M. T. Phase behaviour and composition in the formamidinium−methylammonium hybrid lead iodide perovskite solid solution. *J. Mater. Chem. A* **2016**, *4*, 15375−15382.
(25) Grancini, G.; Marras, S.; Prato, M.; Giannini, C.; Quarti, C.; De Angelis, F.; De Bastiani, M.; Eperon, G. E.; Snaith, H. J.; Manna, L.; et al. The impact of the crystallization processes on the structural and optical properties of hybrid perovskite films for photovoltaics. *J. Phys. Chem. Lett.* **2014**, *5*, 3836−3842.
(26) Quarti, C.; Grancini, G.; Mosconi, E.; Bruno, P.; Ball, J. M.; Lee, M. M.; Snaith, H. J.; Petrozza, A.; Angelis, F. D. The Raman spectrum of the $CH_3NH_3PbI_3$ hybrid perovskite: interplay of theory and experiment. *J. Phys. Chem. Lett.* **2014**, *5*, 279−284.
(27) Ivanovska, T.; Quarti, C.; Grancini, G.; Petrozza, A.; De Angelis, F.; Milani, A.; Ruani, G. Vibrational Response of Methylammonium Lead Iodide: From Cation Dynamics to Phonon−Phonon Interactions. *ChemSusChem* **2016**, *9*, 2994−3004.
(28) Sanehira, E. M.; Tremolet de Villers, B. J.; Schulz, P.; Reese, M. O.; Ferrere, S.; Zhu, K.; Lin, L. Y.; Berry, J. J.; Luther, J. M. Influence of Electrode Interfaces on the Stability of Perovskite Solar Cells: Reduced Degradation Using MoOx/Al for Hole Collection. *ACS Energy Lett.* **2016**, *1*, 38−45.


DOI: 10.1021/acsenergylett.7b00112
*ACS Energy Lett.* 2017, 2, 802−806